Progress In Electromagnetics Research Letters, Vol. 109, 9–14, 2023

Comb-Shaped Structure Loaded Defected Ground Structure and Its Application in Low-Pass Filters

Junbao Du, Chuan-Min Wang, Lin Li*, and Xian-Chuang Su

Abstract—A new defected ground structure (DGS) with two transmission zeros is presented for the first time by loading a conventional dumb-bell-shaped (DBS) DGS with a comb-shaped structure. Equivalent circuits are developed, and electric parameter extraction is derived. The low-pass filter (LPF) design method based on the proposed new DGS is given. The fabricated filter demonstrates a sharp, wide, and high stopband rejection with an ultra-wide 20 dB rejection bandwidth of $21.9 f_c$, and the sharp attenuation rate is more than 129.4 dB/GHz.

1. INTRODUCTION

Defected ground structures (DGSs) are promising candidates for many components owing to their inherent stopband and compact size [1–4]. DGSs are also utilized in low-pass filter designs [5–10]. In [5], dumb-bell-shaped (DBS) DGSs are employed to develop LPFs. Interdigital_DGSs [6] and split ring type DGSs [7] are also proposed to design LPFs. These new DGS LPFs in [5–7] have considerably wider and deeper stopband characteristics than those of conventional LPFs. However, these LPFs are difficult to achieve both a sharp and wide stopband based on these DGSs in [5–7], which have only one transmission zero. In [8], an LPF with sharp and wide stopband is developed by combining DGSs, uniform impedance stubs and stepped-impedance stubs, and yet the design complexity is increased largely. In [9, 10], two DGSs with two transmission zeros are proposed. However, the DGS LPFs in [9, 10] have a narrower stopband because the zero separation is not large enough.

In this letter, a new defected structure (DGS) is presented. Theoretical analysis based on equivalent circuit is carried out, and corresponding electric parameter extraction methods are developed. It is found that the proposed DGS has two transmission zeros, and the zero location can be tuned flexibly to produce both a sharp and wide stopband. Finally, an exemplary LPF is designed, and the experimental results agree well with the simulations.

2. THE PROPOSED DGS AND ITS APPLICATION IN LPF DESIGN

2.1. The Proposed DGS and Its Equivalent Circuit

The proposed comb-shaped structure loading a dumb-bell-shaped DGS is presented in Figure 1(a). Figure 1(b) shows the HFSS-simulated S-parameters of the proposed DGS. As shown in Figure 1(b), the new DGS exhibits different response characteristics from the conventional DBS-DGS once the comb-shaped structures are loaded. Two transmission zeros and one transmission pole appear in the response of the new DGS.

Received 14 November 2022, Accepted 18 January 2023, Scheduled 27 January 2023
* Corresponding author: Lin Li (lilin_door@hotmail.com).
The authors are with the Key Laboratory of Intelligent Textile and Flexible Interconnection of Zhejiang Province, Zhejiang Sci-Tech University, Hangzhou, Zhejiang 310018, China.

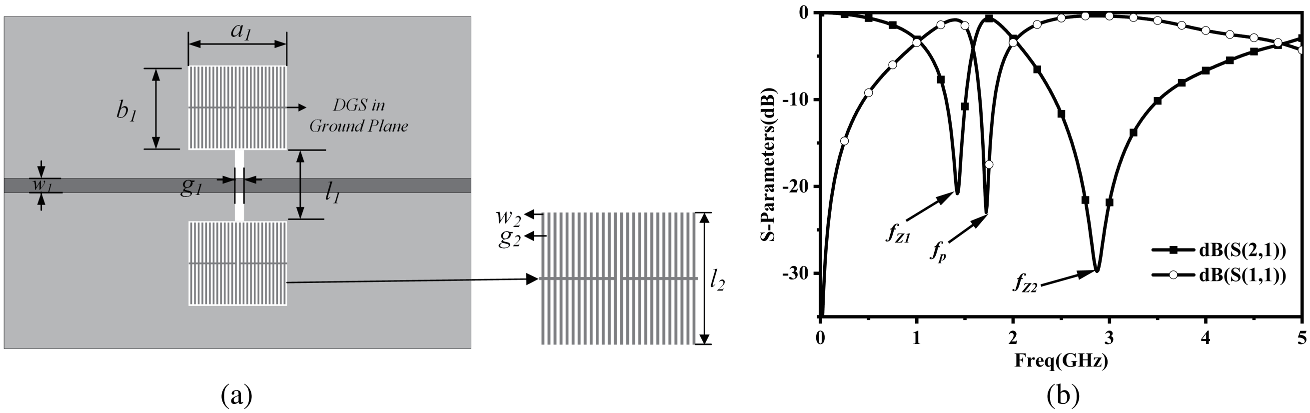

Figure 1. (a) The proposed DGS. (b) Simulated S-parameters. The dimension is $w_1 = 1.5\,\text{mm}$, $g_1 = 0.5\,\text{mm}$, $l_1 = 5.5\,\text{mm}$, $a_1 = b_1 = 12\,\text{mm}$, $g_2 = 0.2\,\text{mm}$, $1_2 = 11.6\,\text{mm}$, $w_2 = 0.25\,\text{mm}$, respectively. The 0.8-mm-thick FR4 with the dielectric constant of 4.4 was used for all cases.

Moreover, zero frequencies can be adjusted by changing the dimension of the periodic comb-shaped structure. Figure 2(a) compares the simulated responses of the proposed DGSs with different periodical numbers N. As shown in Figure 2(a), both transmission zeros are drawn to the lower area when N increases. Furthermore, the comb length l_2 can also be adjusted to change the transmission zero position. In order to continuously inspect the effects of l_2 on the response, a comparison has been made with different l_2 in Figure 2(b). Similarly, both transmission zeros are pushed to the lower side when a larger l_2 is utilized.

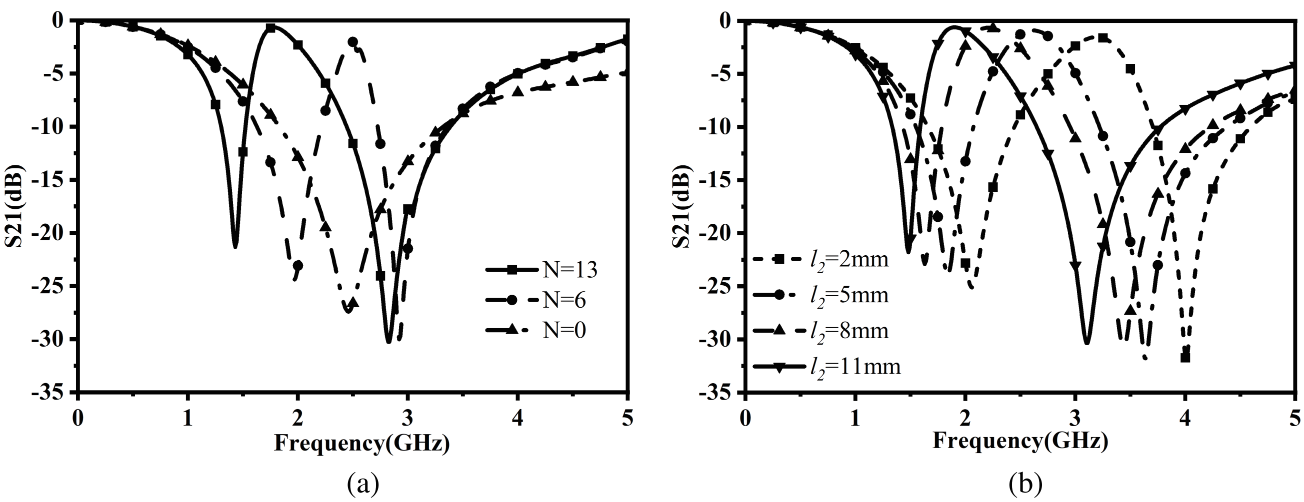

Figure 2. Simulated S_{21} with different parameters. (a) Periodical number N. (b) Comb length l_2.

Additionally, due to its double band gap characteristic, the proposed DGS can be described by the equivalent circuit in Figure 3(a), where C_{S1} represents the capacitance of the narrow slit in the DGS; C_{S2} represents the capacitance brought by the loaded comb shaped structure; and L_{S1} and L_{S2} represent the inductance caused by the rectangular lattice on the two sides of the comb-shaped structure loaded position. The reactance X_{DGS} of the proposed DGS in Figure 3(a) can be expressed by the following formula:

$$X_{\text{DGS}} = \frac{(L_{S1} + L_{S2}) - \omega^2 L_{S1} L_{S2} C_{S2}}{\omega^4 L_{S1} L_{S2} C_{S1} C_{S2} - \omega^2 (L_{S1} C_{S1} + L_{S2} C_{S1} + L_{S2} C_{S2}) + 1} \tag{1}$$

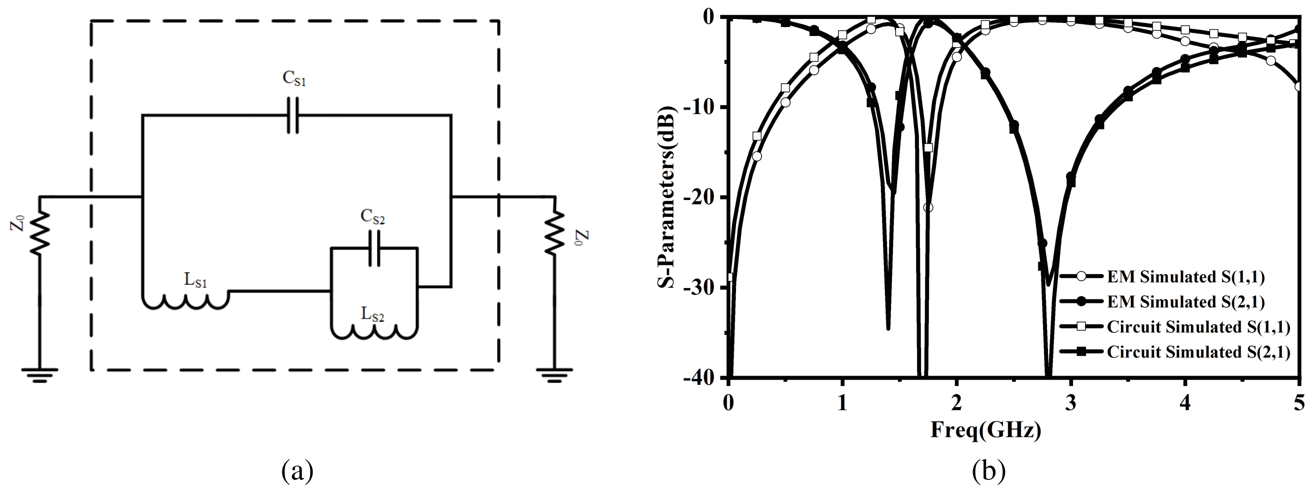

Figure 3. (a) Equivalent circuit. (b) EM Simulated and circuit simulated S parameters.

Obviously, $S_{21} = 0$ when $X_{\mathrm{DGS}} = \infty$. It can be derived from (1) that the two transmission zeros frequencies of ω_{Z1} and ω_{Z2} must satisfy the following relationship:

$$\omega_{Z1}^2 + \omega_{Z2}^2 = \frac{1}{L_{S1}L_{S2}C_{S1}C_{S2}}(L_{S1}C_{S1} + L_{S2}C_{S1} + L_{S2}C_{S2}) \quad (2)$$

$$\omega_{Z1}^2\omega_{Z2}^2 L_{S1}L_{S2}C_{S1}C_{S2} = 1 \quad (3)$$

Obviously, $S_{21} = \infty$ when $X_{\mathrm{DGS}} = 0$. So, the transmission pole frequency of ω_p can be calculated from (1) as:

$$\omega_P = 2\pi f_P = \sqrt{\frac{L_{S1} + L_{S2}}{L_{S1}L_{S2}C_{S2}}} \quad (4)$$

DGSs are always employed to replace inductors for the DGS LPF. Consequently, the equivalent reactance of the proposed DGS should be equal to that of the replaced inductor at the cut-off frequency of ω_c. So

$$X_{DGS,\omega=\omega_c} = \omega_c L_k \quad (5)$$

where L_k is the inductance of the inductor replaced by the proposed DGS.

By combining formulas of (1)–(5), all the element values of the equivalent circuit in Figure 3(a) can be extracted if ω_{Z1}, ω_{Z2}, ω_p, ω_c, and L_k are predetermined. The calculated element values of the proposed DGS in Figure 3(a) are $L_{S1} = 8.50\,\mathrm{nH}$, $L_{S2} = 3.00\,\mathrm{nH}$, $C_{S1} = 0.44\,\mathrm{pF}$, and $C_{S2} = 3.73\,\mathrm{pF}$, respectively. Figure 3(b) shows a good agreement between the EM simulation and equivalent circuit simulation results, which verifies the validity of the circuit model.

2.2. Low-Pass Filter Design

Here is a seven-pole LPF operating at a ω_c of 0.9 GHz with the 0.01 dB ripple level which is discussed below.

Firstly, the LC circuit is given in Figure 4. The values of C_1, C_3, C_5, C_7, L_2, L_4, and L_6 can be calculated from Equations (6) and (7) according to filter theory.

$$L_i = \frac{g_i Z_0}{\omega_c} \quad (6)$$

$$C_i = \frac{g_i}{\omega_c Z_0} \quad (7)$$

Here g_i ($i = 1, 2, 3, 4, 5, 6, 7$) is the normalized component value of the low-pass filter.

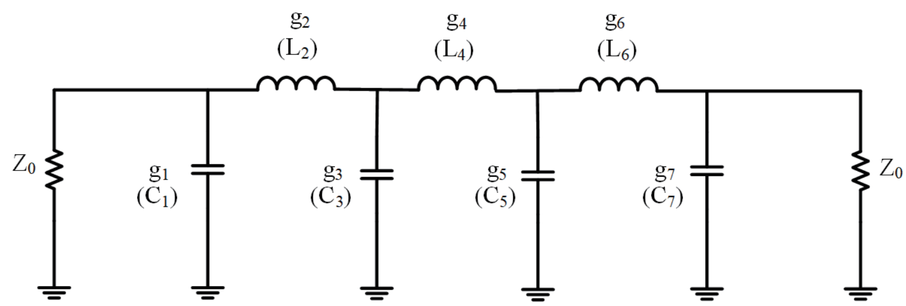

Figure 4. Seven-pole Chebyshev prototype LPF.

Secondly, DGSs are utilized to realize the inductors in Figure 4. If all three inductors are implemented with the proposed DGSs, the stopband will deteriorate owing to the fluctuation around ω_P. Consequently, only the middle inductor is replaced by the proposed DGS, and then the equivalent circuit in Figure 4 is transformed to that in Figure 5.

Next, LC values of the DGSs are calculated. The values of L_{S1}, L_{S2}, C_{S1}, and C_{S2} are obtained

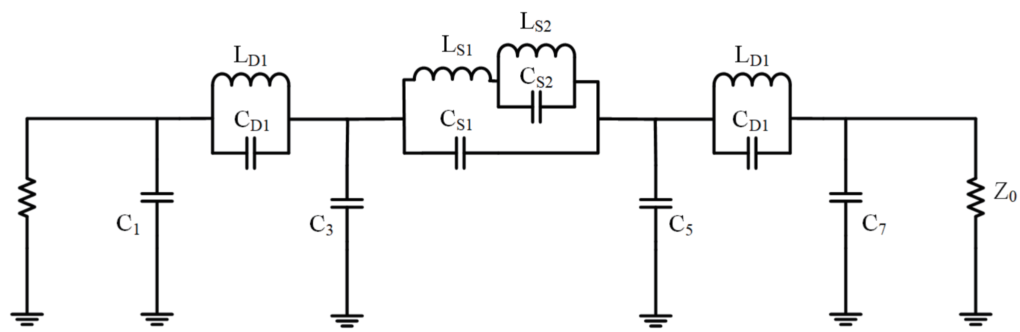

Figure 5. Modified seven-pole prototype LPF.

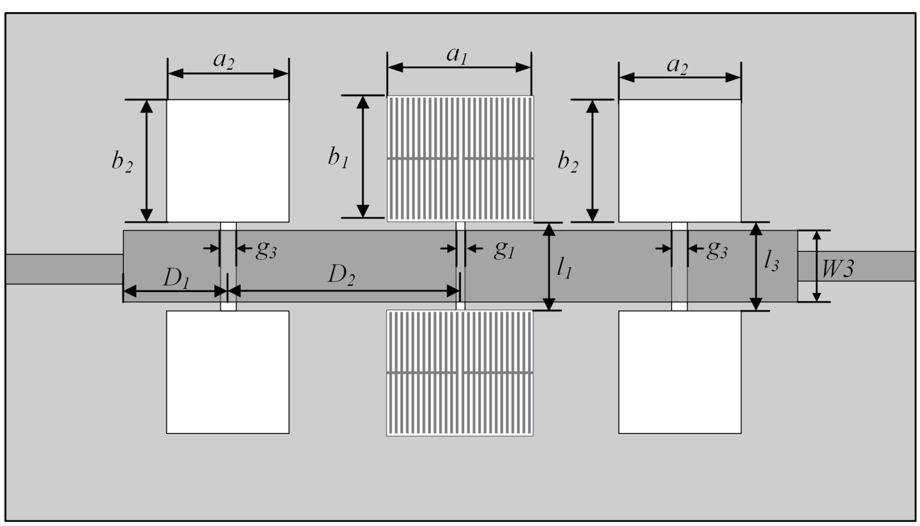

Figure 6. The layout of the exemplary LPF.

from Equations (1)–(5). The values of L_{D1} and C_{D1} are calculated according to the following formula:

$$L_{D1} = \frac{1}{\omega_0^2 C_{D1}} \tag{8}$$

$$\frac{1}{\omega_c L_2} = \frac{1}{\omega_c L_{D1}} - \omega_c C_{D1} \tag{9}$$

where ω_0 is the transmission zero frequency of the DBS-DGS.

Let $f_{Z1} = 1.4\,\text{GHz}$, $f_{Z2} = 2.8\,\text{GHz}$, $f_P = 1.75\,\text{GHz}$, and $f_0 = 2.5\,\text{GHz}$, and Table 1 gives the calculated values of all the electrical elements in Figure 4 and Figure 5. The four shunt capacitors in Figure 5 are realized by the low-impedance lines between DGS patterns in Figure 6. The layout dimension is obtained as: $a_1 = b_1 = 12\,\text{mm}$, $a_2 = b_2 = 11.6\,\text{mm}$, $g_1 = 0.5\,\text{mm}$, $g_2 = 0.2\,\text{mm}$, $g_3 = 1\,\text{mm}$, $l_1 = l_3 = 5.5\,\text{mm}$, $l_2 = 11.6\,\text{mm}$, $w_1 = 1.5\,\text{mm}$, $w_2 = 0.25\,\text{mm}$, $w_3 = 5.5\,\text{mm}$, $D_1 = 15\,\text{mm}$, $D_2 = 24\,\text{mm}$.

Table 1. Calculated values of all the circuit parameters.

Parameters	Values	Parameters	Values	Parameters	Values	Parameters	Values
C_1, C_7	3.37 pF	L_2, L_6	14.05 nH	L_{S1}	8.31 nH	C_{S2}	3.64 pF
C_3, C_5	7.16 pF	L_4	16.35 nH	L_{S2}	3.06 nH	C_{D1}	0.42 pF
C_{S1}	0.47 pF	L_{D1}	12.18 nH				

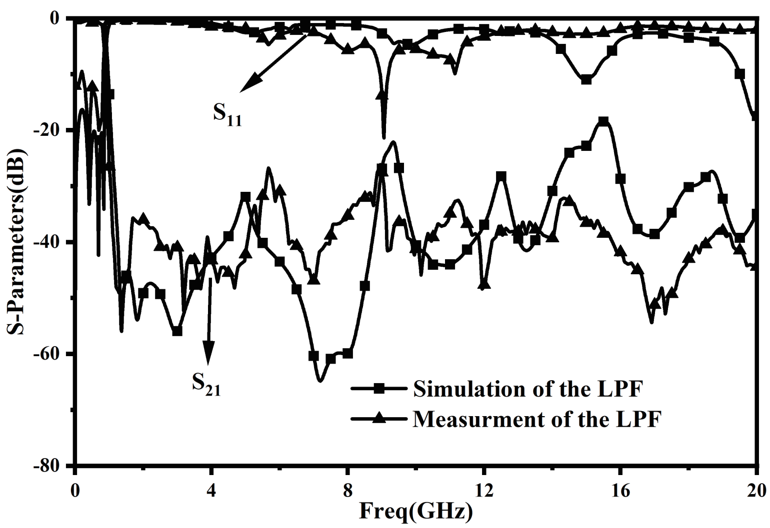

(a)

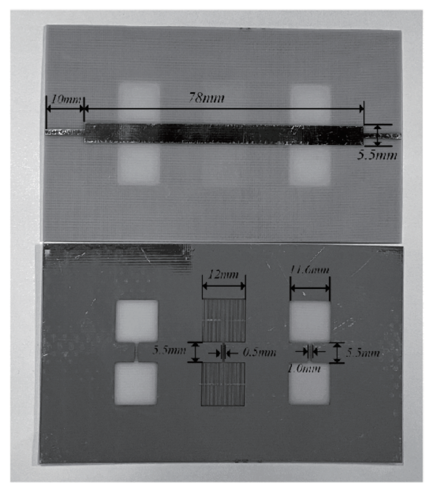

(b)

Figure 7. (a) Simulated and measured S_{21} and S_{11}. (b) Top and bottom view of the filter.

3. EXPERIMENTAL RESULTS

Figure 6 shows the layout of the designed LPF. Figure 7(a) shows the HFSS simulated and measured S-parameters of the fabricated LPF. The simulated 3 dB passband extends to 0.9 GHz with $|S_{11}|$ higher than 18 dB, while the measured one extends to 0.87 GHz with $|S_{11}|$ higher than 11 dB. The simulated roll-off at the transition knee is 129.4 dB/GHz while the measurement is 129.4 dB/GHz. The simulated 20 dB rejection stopband ranges from 1.04 GHz to 20.0 GHz while the measurement ranges from 0.97 GHz to 20.0 GHz. In conclusion, the simulated and measured results of the filter are in good agreement, with good in-band and out-of-band characteristics. Figure 7(b) shows a photograph of the filter. The size of the LPF is $0.071\lambda_g^2$, where λ_g is the microstrip line guided wavelength at the cut-off frequency.

Table 2. Comparison with the low-pass filter in the paper.

Reference	Cut-off Frequency (GHz)	Size (λ_g^2)	Roll-Off dB/GHz)	Stop-Band FBW (20 dB)
[6]	3.00	0.026	16.5	$1.9f_c$
[7]	3.37	0.036	188.7	$1.7f_c$
[8]	1.00	0.016	78.0	$18.1f_c$
[9]	4.00	0.285	130.0	$4.7f_c$
[10]	1.90	0.030	75.0	$5.3f_c$
This work	0.87	0.071	129.4	$21.9f_c$

Table 2 compares the proposed LPF with several reported high-performance DGS LPFs. Compared with other LPFs, the proposed LPF has the widest stopband and a sharper transition except that in [7]. So, the proposed LPF exhibits both a sharp and wide stopband.

4. CONCLUSIONS

A DGS with a comb-shaped structure is presented. In comparison with other DGSs, it has two tunable transmission zeros. Thus, both a sharp and wide stopband can be achieved for LPFs based on the proposed DGS. The designed LPF has been tested, and the measurement agrees well with the simulation, proving the feasibility of the proposed DGS.

REFERENCES

1. Ponchak, G. E., "Dual of defected ground structure for coplanar stripline," *IEEE Microw. Wireless Compon. Lett.*, Vol. 18, No. 2, 105107, Feb. 2018.
2. Yi, Z. and C. Wang, "Noninvasive glucose sensors using defective-ground-structure coplanar waveguide," *IEEE Sens. J.*, Vol. 23,, No. 1, 195201, Jan. 2023.
3. Liu, Y.-T., K. W. Leung, and N. Yang, "Compact absorptive filtering patch antenna" *IEEE Trans. Antennas Propag.*, Vol. 68,, No. 2, 633–642, Feb. 2020.
4. Liu, Y., X. Yang, Y. Jia, et al., "A low correlation and mutual coupling MIMO antenna," *IEEE Access*, Vol. 7, 127384127392, Sep. 2019.
5. Lim, J.-S., C.-S. Kim, D. Ahn, et al., "Design of low-pass filters using defected ground structure," *IEEE Trans. Microw. Theory Tech.*, Vol. 53,, No. 8, 2539–2545, Aug. 2005.
6. Balalem, A., A. R. Ali, J. Machac, et al., "Quasi-elliptic microstrip low-pass filters using an interdigital DGS slot," *IEEE Microw. Wireless Compon. Lett.*, Vol. 17,, No. 8, 586–588, Aug. 2007.
7. Xiao, M., G. Sun, and X. Li, "A lowpass filter with compact size and sharp roll-off," *IEEE Microw. Wireless Compon. Lett.*, Vol. 25, No. 12, 790–792, Dec. 2015.
8. Chen, F., H. Hu, J. Qiu, and Q. Chu, "High-selectivity low-pass filters with ultrawide stopband based on defected ground structures," *IEEE Trans. Microw. Theory Tech.*, Vol. 5,, No. 9, 1313–1319, Sept. 2015.
9. Chen, Q. and J. Xu, "DGS resonator with two transmission zeros and its application to lowpass filter design," *Electron. Lett.*, Vol. 46, No. 21, Oct. 2010.
10. Cao, S., Y. Han, H. Chen, and J. Li, "An ultra-wide stop-band LPF using asymmetric pi-shaped koch fractal DGS," *IEEE Access*, Vol. 5, 27126–27131, Nov. 2017.